

High-Resolution ^{13}C and ^{15}N NMR Investigations of the Mechanism of the Curing Reactions of Cyanate-Based Polymer Resins in Solution and the Solid State

C. A. Fyfe,* J. Niu, S. J. Rettig, and N. E. Burlinson

Department of Chemistry, University of British Columbia, Vancouver, British Columbia, Canada V6T 1Z1

C. M. Reidsema, D. W. Wang, and M. Poliks

Systems Technology Division, IBM Corporation, 1701 North Street, Endicott, New York 13760

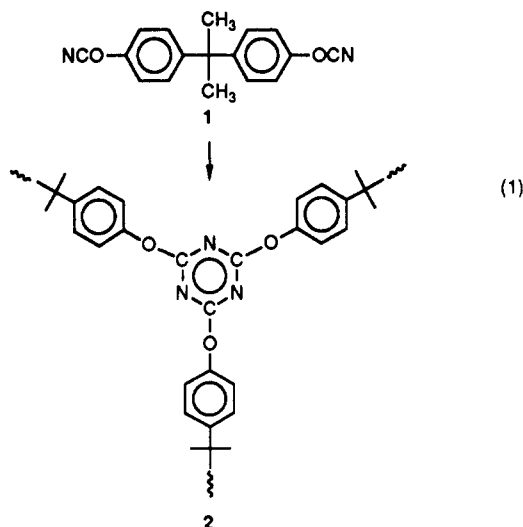
Received January 23, 1992; Revised Manuscript Received June 1, 1992

ABSTRACT: The mechanism of the curing reactions of cyanate polymer resins based on Bisphenol A dicyanate has been investigated both in solution and in the solid state by NMR spectroscopic techniques. To increase *S/N* and to unambiguously characterize the reactions of the cyanate functionalities, ^{13}C - and ^{15}N -enriched cyanate resins and monocyanate model compounds were used, the latter yielding soluble and isolable analogs. In solution, the main reaction is formation of triazine rings as identified by NMR and MS techniques and characterized by single-crystal X-ray diffraction on an isolated crystalline compound from the monocyanate model compound. Side products are formed by the reaction of the cyanate functionalities with trace water present in the solvent but there is no NMR evidence for the formation of dimeric or other intermediate species prior to triazine ring formation. The isolated resins from the solution curing and also those formed directly by heat curing of the neat resin were characterized by high-resolution solid-state NMR. In the former case triazine ring formation and the presence of side products were confirmed by both ^{13}C and ^{15}N solid-state NMR and their proportions quantified. In the case of the neat resin, the curing reaction is shown to be almost quantitative. This is rationalized in terms of the very strong intermolecular intercyanate bonding interactions observed in the crystal structure of the Bisphenol A dicyanate monomer obtained from a single-crystal X-ray diffraction experiment.

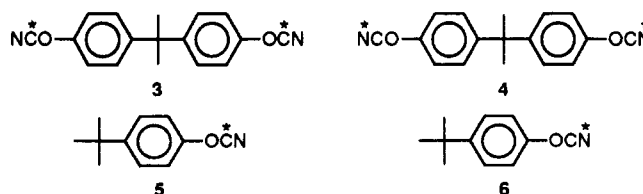
Introduction

The cyanate resins are commonly derived from the Bisphenol A type of monomer. The cured resins exhibit good thermal, mechanical, and insulating characteristics and have been considered for many electronic packaging and structural materials applications.¹⁻⁴

Bisphenol A dicyanate (BPACN, 1) is one of the resins most often used. The curing reaction is postulated to proceed by reaction of three cyanate (OCN) groups to form a triazine ring (2) as in eq 1. The curing is known



of model systems have been studied and IR investigations carried out to identify some of the functionalities during curing,^{5,6} there is little direct evidence to date regarding the species involved or the nature and efficiency of the curing process itself. Fang has recently described the use of ^{13}C solution NMR to determine the molecular weights of BPACN oligomers.⁷ The purpose of the present work was to carry out an exploratory investigation of the curing reactions of these resins by high-resolution ^{13}C and ^{15}N NMR spectroscopy in both solution and the solid state. To facilitate these studies and to cleanly monitor the reactive functional groups during the curing process, dicyanate monomers enriched in ^{13}C (3) and ^{15}N (4) were used. This facilitates observation of the cyanate group reactions by minimizing the contributions of the other parts of the molecule to the spectra. In addition, to provide good reference materials for the identification of reaction products, the reactions of the analogous monocyanates (5 and 6), where cross-linking will not occur during triazine formation, have also been studied.



Experimental Section

NMR Spectra. High-resolution ^{13}C and ^{15}N NMR spectra were obtained using Varian XL300 and Bruker ACE200 spectrometers. Deuterated solvents used were from commercial

to take place in the presence or absence of catalyst and both in solution and in the bulk. Although the reactions

Table I
Crystallographic Data^a for the Triazine 9

formula	C ₃₃ H ₃₉ N ₃ O ₃
fw	525.69
cryst system	monoclinic
space group	P2 ₁ /c
a, Å	12.214 (2)
b, Å	6.556 (2)
c, Å	37.981 (2)
β, deg	90.644 (7)
V, Å ³	3041 (1)
Z	4
D _c , g/cm ³	1.148
F(000)	1128
μ(Cu Kα), cm ⁻¹	5.50
cryst dims, mm	0.25 × 0.30 × 0.45
transmission factors	0.95–1.00
scan type	ω – 2θ
scan range, deg in ω	1.05 + 0.20 tan θ
scan speed, deg/min	32
data collected	+h, –k, ±l
2θ _{max} , deg	158.3
cryst decay	negligible
total reflections	7245
unique reflections	6940
R _{merge}	0.021
no. of reflns with I ≥ 3σ(I)	4220
no. of variables	380
R	0.042
R _w	0.057
GOF	1.99
max Δ/σ (final cycle)	0.11
residual density, e/Å ³	–0.17 to +0.19

^a Temperature 294 K, Rigaku AFC6S diffractometer, Cu radiation (λ = 1.54178 Å), graphite monochromator, takeoff angle 6.0°, aperture 6.0 × 6.0 mm at a distance of 285 mm from the crystal, stationary background counts at each end of the scan (scan/background time ratio 2:1), σ²(F²) = [C + B + (0.03F²)²]/Lp² (C = scan count, B = normalized background count), function minimized Σw(|F_o| – |F_c|)² where w = 4F_o²/σ²(F²), R = Σ||F_o| – |F_c||/Σ|F_o|, R_w = (Σw(|F_o| – |F_c|)²/Σw|F_o|²)^{1/2}, and GOF = [Σw(|F_o| – |F_c|)²/(m – n)]^{1/2}. Values given for R, R_w, and GOF are based on those reflections with I ≥ 3σ(I).

sources, and the ¹³C and ¹⁵N chemical shifts are given with respect to TMS and neat formamide, respectively. ¹³C and ¹⁵N CP MAS solid-state NMR spectra were obtained using Bruker CXP 100 and MSL 400 spectrometers using commercial double-resonance probes with the magic angle set using the ⁷⁹Br resonance of KBr.⁸

X-ray Crystallographic Analysis of 9. Crystallographic data appear in Table I. The final unit-cell parameters were obtained by least squares on the setting angles for 25 reflections with 2θ = 59.3–96.0°. The intensities of three standard reflections, measured every 200 reflections throughout the data collection, showed only small random variations. The data were processed⁹ and corrected for Lorentz and polarization effects and absorption (empirical, based on azimuthal scans for three reflections).

The structure was solved by direct methods, the coordinates of the non-hydrogen atoms being determined from an E-map. One of the *tert*-butyl groups exhibited 2-fold orientational disorder. A split-atom model was employed, the site occupancy factors being refined as the isotropic stage of the analysis (with the constraint that the average thermal parameters for the atoms of each component are equal). In the final stages of refinement the site occupancy factors were kept fixed at the previously determined values. All non-hydrogen atoms (including the disordered carbon atoms) were refined with anisotropic thermal parameters. Hydrogen atoms were fixed in calculated positions (C–H = 0.98 Å, B_H = 1.2B_{bonded atom}). A secondary extinction correction was applied, the final value of the extinction parameter being 2.84 × 10⁻⁶. Neutral atom scattering factors and anomalous dispersion corrections for the non-hydrogen atoms were taken from the *International Tables for X-Ray Crystallography*.¹⁰ Final atomic coordinates and equivalent isotropic thermal parameters, bond lengths, and bond angles are given in Tables II–IV, respectively.

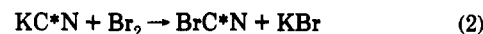
X-ray Crystallographic Analysis of Bisphenol A Dicyanate. Crystallographic data from the X-ray crystallographic

analysis of Bisphenol A dicyanate (BPACN, 1) appear in Table VI. The final unit-cell parameters were obtained by least squares on the setting angles for 25 reflections with 2θ = 20.0–26.1°. The intensities of three standard reflections, measured every 200 reflections throughout the data collection, remained essentially constant. The data were processed⁹ and corrected for Lorentz and polarization effects and absorption (empirical). A total of 2875 reflections with 2θ ≤ 50° was collected on a Rigaku AFC6S diffractometer. Of these, 2714 were unique (R_{int} = 0.025), and, of those, 1307 having I ≥ 3σ(I) were employed in the solution and refinement of the structure.

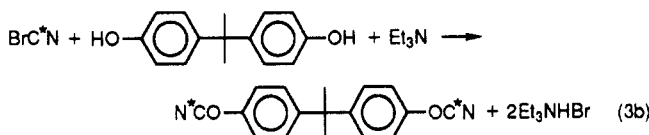
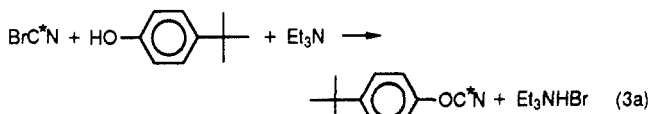
The structure was solved by direct methods, the coordinates of the non-hydrogen atoms being determined from an E-map. The non-hydrogen atoms were refined with anisotropic thermal parameters. The hydrogen atoms were fixed in idealized positions (C–H = 0.98 Å, B_H = 1.2B_{bonded atom}). A correction for secondary extinction was applied, the final value of the extinction coefficient being 7.78 × 10⁻⁵. Neutral atom scattering factors and anomalous dispersion corrections for all atoms were taken from the *International Tables for X-Ray Crystallography*.¹⁰ Final atomic coordinates and equivalent isotropic thermal parameters are given in Table VII.

A more detailed listing of crystallographic data, hydrogen atom parameters, anisotropic thermal parameters, bond lengths, bond angles, torsion angles, intermolecular contacts, least-squares planes, and measured and calculated structure factor amplitudes is included as supplementary material for both structures.

Syntheses. The ¹³C- and ¹⁵N-enriched monomers were synthesized by a two-step procedure. First, the labeled cyanogen bromide (Br¹³CN or BrC¹⁵N) was made by using either K¹³CN or KC¹⁵N as the labeled starting material (eq 2), following a procedure similar to that of Hartman and Dreger.¹¹ The labeled



cyanogen bromides were then reacted with the appropriate phenol to produce the final labeled cyanate compounds (eq 3). Detailed synthesis procedures are given below and are modifications of literature methods.¹²



(1) Labeled Cyanogen Bromide (BrC*_N). A total of 0.50 mL of Br₂ (0.01 mol) and 0.5 mL of H₂O are added to a 25-mL round-bottomed flask fitted with a magnetic stirring bar, sitting in an ice–water bath. To the stirred mixture is added dropwise from a pipet over a 20-min period a solution of 0.65 g (0.01 mol) of labeled KC*_N dissolved in 2 mL of H₂O. The exact amount of KC*_N solution needed to titrate the system just to a colorless or light yellow end point is added. The purification step can be performed immediately after BrCN formation. The distillation is conducted at room temperature under vacuum with a dry ice–acetone trap as a product collector. The final BrCN product is a white crystalline solid, yield = 70–75%.

(2) Labeled BPACN: 3 and 4. A 50-mL round-bottomed flask fitted with a pressure-equalizing dropping funnel and a magnetic stirring bar, sitting in an ice–water bath, is charged with 1.10 g (0.0105 mol) of BrC*_N and a solution of 1.14 g (0.005 mol) of Bisphenol A in 10 mL of acetone. The mixture is stirred rapidly with cooling in the ice–water bath while 1.01 g (0.01 mol) of Et₃N is added dropwise over a 20-min period through the dropping funnel. Stirring is continued for 30 min while the mixture warms to room temperature. The product is isolated by slowly pouring the mixture into 50 mL of ice-cooled water with vigorous stirring. The solid is then isolated by filtration and washed with water until a neutral eluant is obtained. After

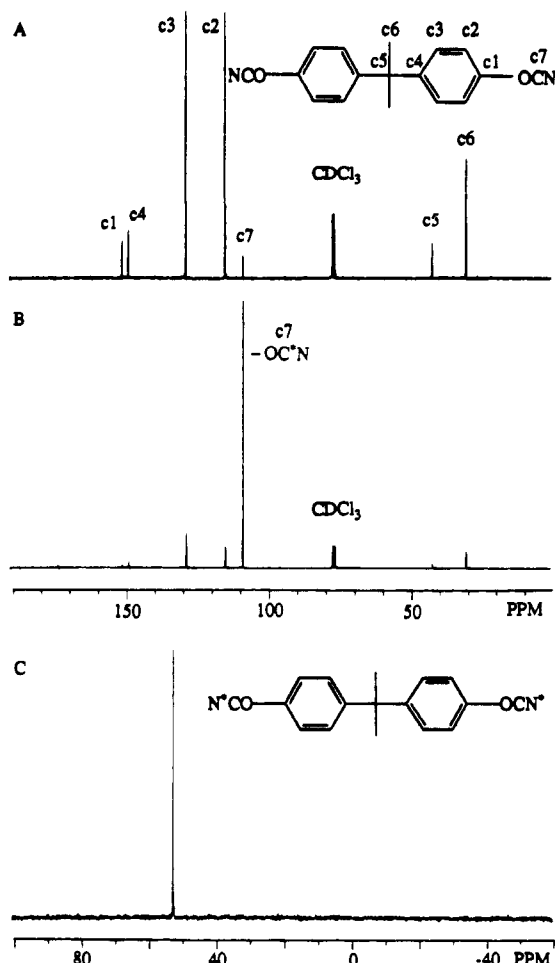


Figure 1. Solution NMR spectra of Bisphenol A dicyanate (BPACN) monomer in CDCl_3 . (A) ^{13}C NMR spectrum of the natural-abundance monomer. (B) ^{13}C NMR spectrum of the ^{13}C -enriched monomer. (C) ^{15}N NMR spectrum of the ^{15}N -enriched monomer.

vacuum drying, the crude product is recrystallized from cyclohexane, mp = 80 °C and yield = 80–85%.

(3) Labeled PTBPCN: 5 and 6. A 50-mL round-bottomed flask equipped with a magnetic stirrer and a pressure-equalizing dropping funnel, sitting in an ice-water bath, is charged with 1.10 g (0.0105 mol) of BrC^*N and a solution of 1.5 g (0.01 mol) of *p*-*tert*-butylphenol in 10 mL of acetone. The mixture is stirred rapidly while in the ice-water bath, and 1.01 g (1.39 mL, 0.01 mol) of Et_3N is added dropwise over a 20-min period through a dropping funnel. After an additional 15 min of stirring, the mixture is warmed to room temperature. The white precipitate of $\text{Et}_3\text{N}^+\text{HBr}^-$ is removed by filtration, and the solvent is then removed by evaporation using a rotary evaporator under reduced pressure at room temperature. The final mixture is distilled under a vacuum of 0.5 mmHg at 75 °C. The final product is a colorless liquid, yield = 76–87%.

(4) Preparation and Isolation of the Triazine Formed from *p*-*tert*-Butylphenyl Cyanate. The triazine is prepared by heating a sample of *p*-*tert*-butylphenyl cyanate in a sealed tube for 2 h at 150 °C. When the sample turns to solid, it can be recrystallized from acetone, and needle-shaped crystals are formed, mp = 193.5 °C. The ^1H and ^{13}C NMR spectra in deuteriochloroform and acetone are in complete agreement with the postulated structure, as is the mass spectrum ($M^+ = 525$).

A small quantity of ^{15}N -labeled material is also synthesized and recrystallized from acetone. The ^{15}N spectrum is again in agreement with the proposed structure and shows no coupling to protons as expected.

Results and Discussion

A. Synthesis and Characterization of Specifically Labeled Monomers (3–6). The ^{13}C - and ^{15}N -enriched

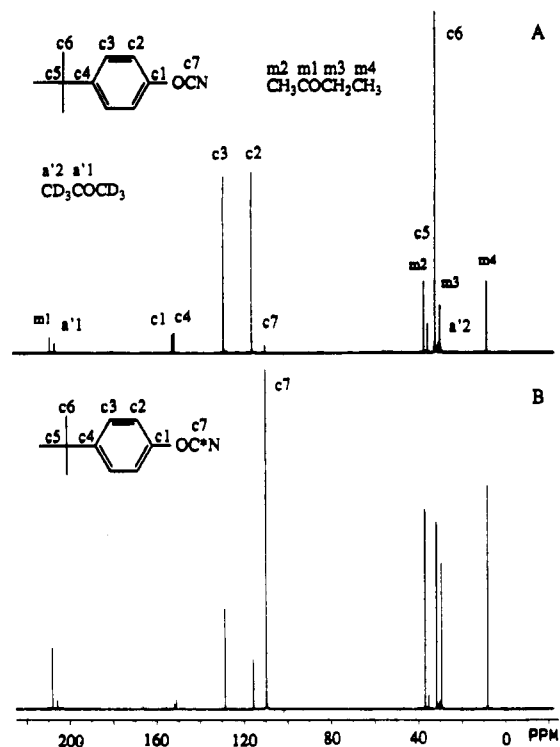
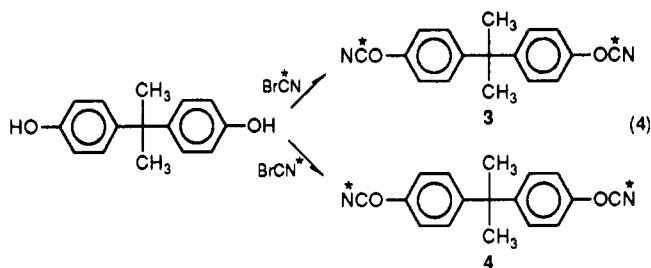


Figure 2. ^{13}C solution NMR spectra of (A) natural-abundance *p*-*tert*-butylphenyl cyanate (PTBPCN) and (B) ^{13}C -enriched PTBPCN in methyl ethyl ketone (MEK) and acetone- d_6 .

dicyanate monomers 3 and 4 were prepared from Bisphenol A by reaction with labeled cyanogen bromide as indicated in eq 4, purified, and characterized. The preparations were carried out with unenriched reagents and a small scale reaction suitable for producing appropriate quantities for NMR studies was optimized before using labelled materials. Detailed preparative procedures are given in the Experimental Section.



Parts A and B of Figure 1 show the ^{13}C solution NMR spectra (referenced to TMS) with assignments for natural-abundance and ^{13}C -enriched BPACN monomers, respectively. The large increase in intensity of the peak at ~ 109 ppm due to the OCN carbon indicates that it will be possible to follow its reaction in the curing process by comparison of the spectra of enriched and unenriched materials.

Figure 1C shows the ^{15}N solution NMR spectrum of the ^{15}N -enriched BPACN monomer (4). The OCN nitrogen is clearly observed at ~ 52 ppm (referenced to neat formamide). The natural-abundance spectrum is not detectable under these conditions. The ^{15}N spectra during curing will thus show signals from the cyanate group and its reaction products.

The labeled monomers 5 and 6 were synthesized by reaction of *p*-*tert*-butylphenol with labeled cyanogen bromide according to eq 5 as described in the Experimental Section. The corresponding unlabeled material was also synthesized in larger quantities by the same method.

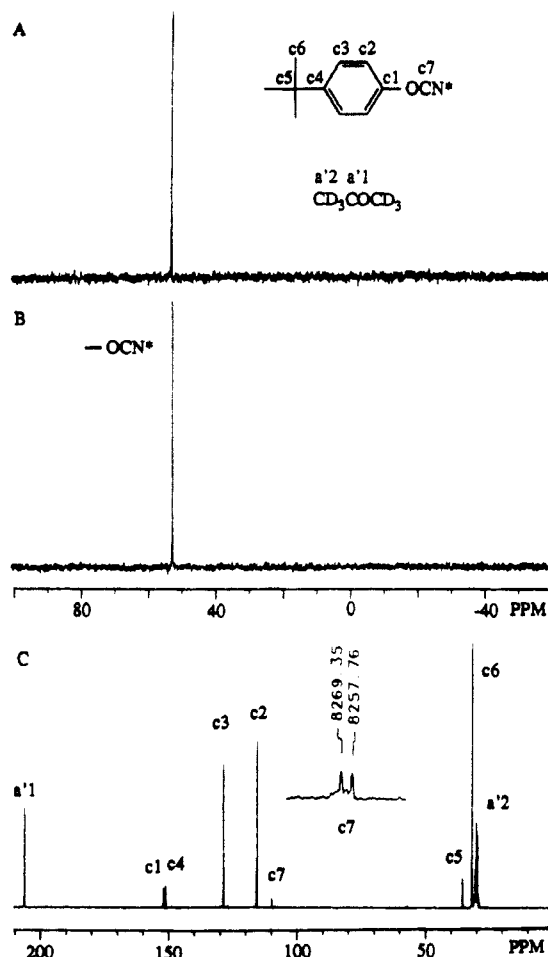


Figure 3. Solution NMR spectra of ^{15}N -enriched PTBPCN in acetone- d_6 . (A) ^{15}N spectrum with ^1H frequency decoupling. (B) ^{15}N spectrum without ^1H frequency decoupling. (C) ^{13}C spectrum with ^1H frequency decoupling.

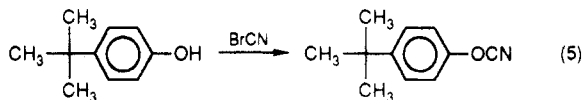


Figure 2A shows the natural-abundance ^{13}C solution NMR spectrum of the cyanate from *p*-*tert*-butylphenol together with the assignment. The corresponding spectrum of the ^{13}C -labeled material, given in Figure 2B, indicates the successful incorporation of ^{13}C into the cyanate group, $\delta = 100$ ppm. Figure 3A shows the ^{15}N spectrum of ^{15}N -labeled cyanate (6). There is a single sharp resonance at ~ 52 ppm consistent with the BPACN spectra, and there are no coupled protons (Figure 3B). The ^{13}C spectrum (Figure 3C) shows a splitting of the OCN resonance, C7, into a doublet due to coupling to the ^{15}N nucleus consistent with the ^{15}N spectrum and confirming the introduction of the ^{15}N nucleus into the cyanate group.

B. Investigation of the Curing Reaction in Solution. ^{13}C NMR Investigation of the Curing Reaction of BPACN in Solution. The progress of the curing reaction in solution was investigated for the ^{13}C -enriched BPACN monomer by high-resolution ^{13}C NMR at a proton frequency of 200 MHz with proton decoupling. The solvent was methyl ethyl ketone (MEK) with a small amount of acetone- d_6 added to provide a deuterium lock signal. Zinc octanoate (200 ppm) was added as a catalyst and the solution heated at 60, 90, and 100 $^\circ\text{C}$ for various times in sealed glass tubes. Representative spectra are given in Figure 4. Figure 4A shows the ^{13}C spectrum of the BPACN monomer before reaction. The three large

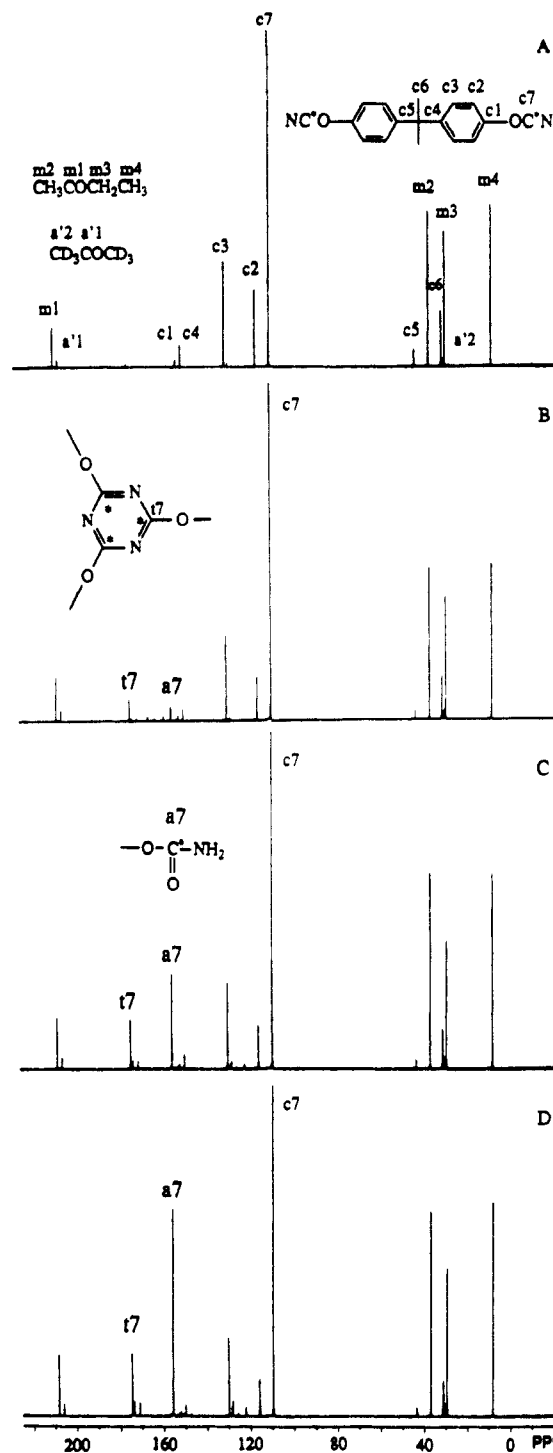


Figure 4. ^{13}C solution NMR spectra of ^{13}C -enriched BPACN in MEK and acetone- d_6 cured with 200 ppm zinc octanoate as catalyst. (A) Before heating. (B) After heating for 1 h at 60 $^\circ\text{C}$. (C) After 16 h at 60 $^\circ\text{C}$. (D) After 5 days at 60 $^\circ\text{C}$.

signals at high field are due to the MEK solvent. The intense signal at 100 ppm is due to the enriched $-\text{O}^{13}\text{C}\equiv\text{N}$ group; it is the behavior of this resonance and those derived from it that is used to monitor the progress of the curing reaction. The other signals in the spectrum are relatively small and agree with those of the unlabeled monomer previously obtained (Figure 1B).

After just 1 h at 60 $^\circ\text{C}$, two new resonances at ~ 157 and 174 ppm are observed (Figure 4B) which grow in intensity with time (Figure 4C,D). These are assigned to the expected triazine (174 ppm) and one other species (157 ppm). The nature of this second species will be discussed in more detail later. Subsequent spectra show the same two major resonances, but their intensities diminish

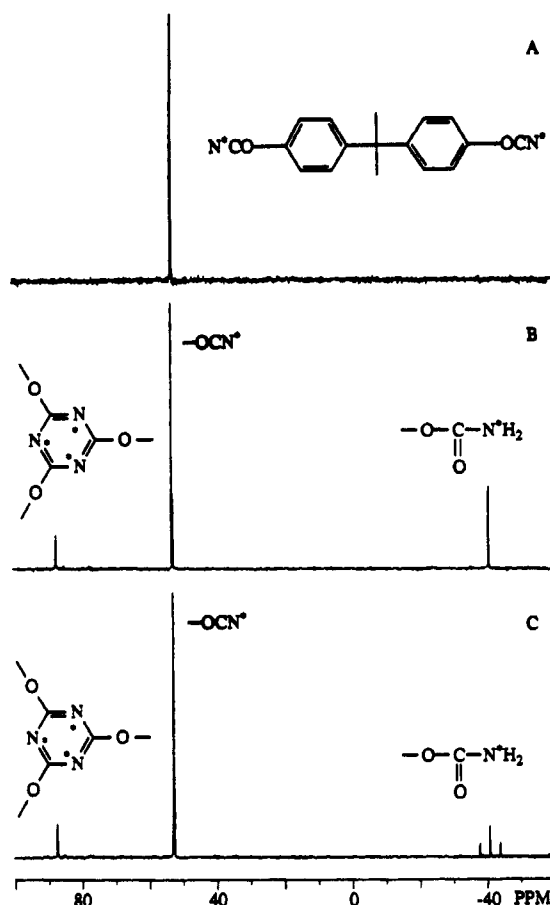


Figure 5. ^{15}N solution NMR spectra of ^{15}N -enriched BPACN in MEK and acetone- d_6 with 200 ppm zinc octanoate as catalyst. (A) Before heating and without ^1H frequency decoupling. (B) After heating at 90°C for 2 days and with ^1H frequency decoupling. (C) Same sample as in B without ^1H decoupling.

relative to those of the solvent signals although the cyanate resonance of the monomer disappears at the same time. This is because the high-resolution spectra detect only the species present in solution: In the curing process taking place while the solution spectra of Figure 4 were obtained, considerable quantities of solid material had precipitated from solution.

^{15}N NMR Investigation of the Curing Reaction of BPACN in Solution. A series of ^{15}N spectra (proton resonance 300 MHz) were obtained under conditions identical to those of the ^{13}C spectra discussed above and are presented in Figure 5. These spectra are particularly informative, as the only signals observed are from the $-\text{OC}^{15}\text{N}$ group and its reaction products, with no interference at all from solvent or unlabeled monomer resonances. The spectra are referenced to the ^{15}N signal from formamide. Figure 5B shows a single sharp signal at ~ 52 ppm as expected, and two additional resonances are observed at -39 ppm and 87 ppm during curing, in agreement with the results from the ^{13}C NMR spectra. The signal at 87 ppm can be assigned to the expected triazine ring (these data are quantitative). Figure 5C was obtained without irradiation of the protons during acquisition, and the signal at -39 ppm shows a triplet structure indicating coupling to two protons while the others are unaffected as expected. These general characteristics are maintained during further curing (spectra not shown) although again a considerable amount of solid material has precipitated and only soluble species are reflected in the solution NMR spectra.

The second product species is postulated to be compound 7 formed by the addition of water to the cyanate

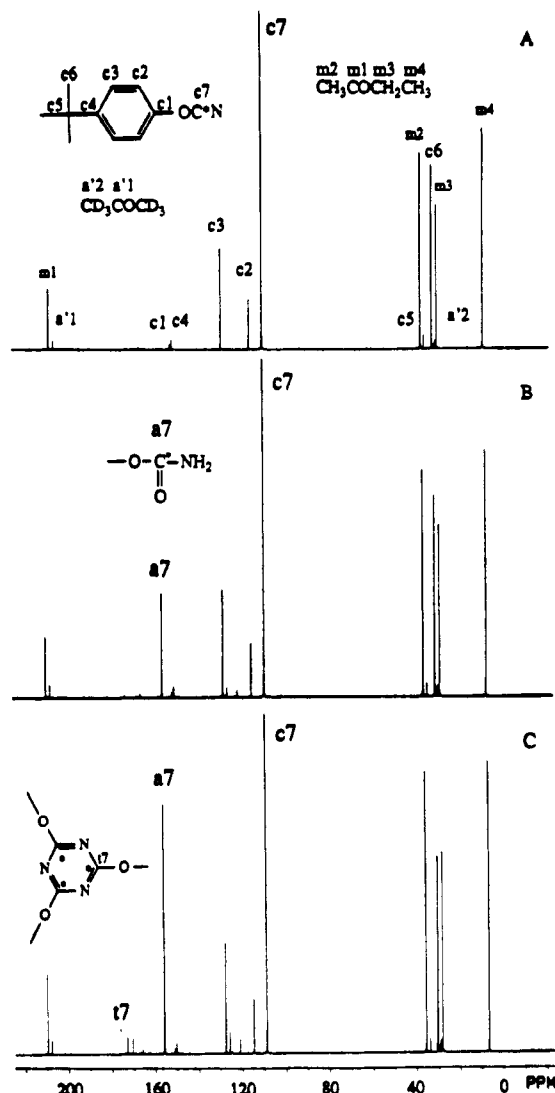
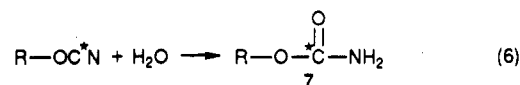


Figure 6. ^{13}C solution NMR spectra of the ^{13}C -enriched PTBPCN in MEK and acetone- d_6 with 200 ppm zinc octanoate as catalyst. (A) Before water addition. (B) After addition of excess water and standing at room temperature for 24 h. (C) After heating at 100°C for 1 h.

group as shown in eq 6.¹³



This structure fits all of the characteristics of the ^{13}C and ^{15}N NMR spectra, particularly the coupling of the ^{15}N nucleus to two protons. Further conformation of the structure of this species is given below. One very important feature of the spectra is that they rule out the formation of substantial amounts of any long-lived intermediate "dimer" species on the route to triazine ring formation. These species would all show two resonances in both their ^{13}C and ^{15}N spectra, and there should be no proton coupling to ^{15}N . Thus the curing reaction appears to be remarkably clean!

^{13}C NMR Investigation of the Reactions of *p*-tert-Butylphenyl Cyanate in Solution. As a complement to the solution NMR studies of BPACN discussed above, the solution reactions of the analogous monocyanate were investigated, with particular emphasis on the identification of the reaction products and the effect of added water. In the case of the monocyanate, no cross-linking can occur and there is no precipitation from the reaction mixture.

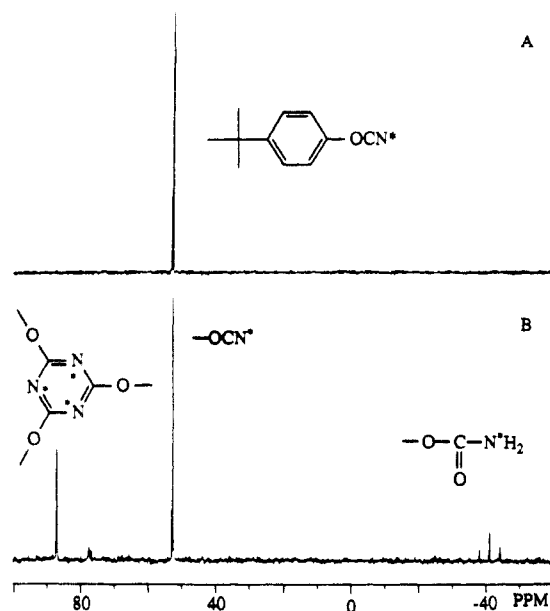
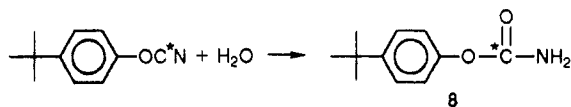


Figure 7. ^{15}N solution NMR spectra of ^{15}N -enriched PTBPCN in MEK and acetone- d_6 without ^1H decoupling. (A) after heating at $100\text{ }^\circ\text{C}$ for 5 h without catalyst. (B) after heating at $100\text{ }^\circ\text{C}$ for 1 h with 200 ppm zinc octanoate as catalyst.

Figure 6A shows the ^{13}C spectrum of the ^{13}C -enriched monomer PTBPCN in MEK solvent, together with its assignment. The large resonance at 109 ppm is due to the cyanate group (C7). An excess of water was added to the system, and it was allowed to stand for 24 h. The OCN resonance is reduced, and a new signal appears at ~ 157 ppm, consistent with the behavior of the dicyanate and assigned to the carbamate (8) in the present instance (Figure 6B). On heating the sample at $100\text{ }^\circ\text{C}$ (Figure 6C), the intensity of this signal increases and small peaks appear at $\delta = 174$ (triazine) and 171 ppm (unknown). On



prolonged heating at $100\text{ }^\circ\text{C}$, the triazine resonance is the major component in the spectrum. Further information on the nature of the other reaction products comes from the ^{15}N spectra (see below).

^{15}N NMR Investigation of the Reactions of *p*-tert-Butylphenyl Cyanate in Solution. An investigation of ^{15}N spectra of PTBPCN in MEK and acetone- d_6 gave results in agreement with the ^{13}C data of the previous section. The experiments were carried out with the ^{15}N -enriched PTBPCN whose spectrum was presented previously in Figure 3. Figure 7A shows that there is no reaction in MEK and acetone without catalyst on heating at $100\text{ }^\circ\text{C}$ for up to 5 h even in the presence of added water. The corresponding ^{13}C spectra which are not shown give the same result. It would appear that trace amounts of catalyst are needed at least at this temperature to induce the reaction. Just as expected, reactions were observed after 200 ppm zinc octanoate was added as catalyst and the sample heated at $100\text{ }^\circ\text{C}$ for only 1 h (Figure 7B). These reactions cause the appearance of two main resonances in the ^{15}N spectrum, one at 87 ppm due to the formation of triazine (9) and a second one at -39 ppm which is split to a triplet due to coupling with two protons. This is consistent with the formation of 8 by the addition of water to the cyanate group as described in the previous section. Two small singlet resonances are also observed due to very small amounts of unknown side products.

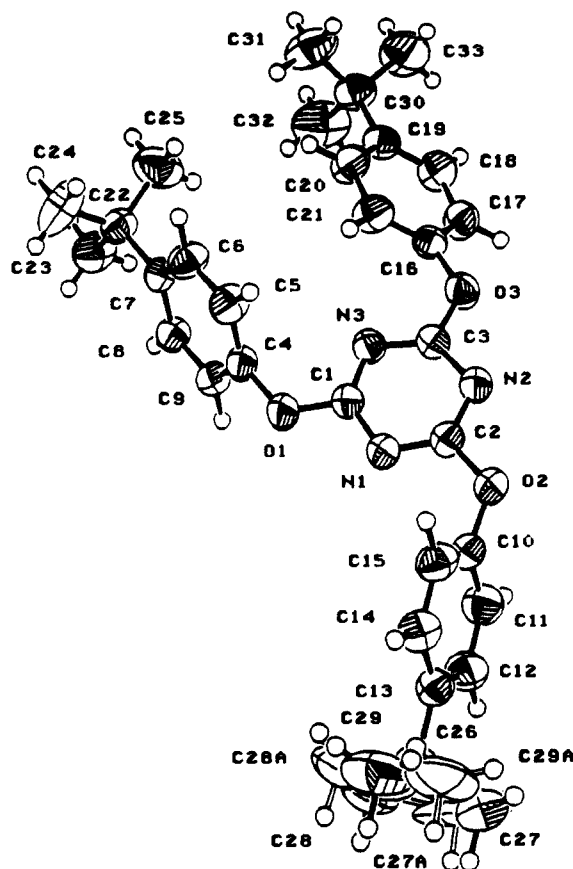
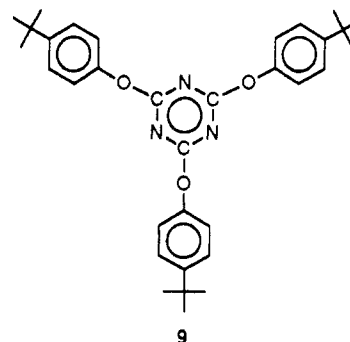


Figure 8. Perspective view of the triazine molecule formed from PTBPCN. 50% probability thermal ellipsoids are shown for the non-hydrogen atoms.

C. Isolation and Characterization of the Triazine from *p*-tert-Butylphenyl Cyanate. Because of the critical importance of triazine ring formation to the cyanate curing process, it was decided to isolate the (anticipated) triazine product from the reaction of *p*-tert-butylphenyl cyanate and thoroughly characterize it to prove that it did indeed have the expected structure 9.



As indicated in the Experimental Section, all of the spectral characteristics were in agreement with both the proposed structure and the ^{13}C and ^{15}N spectra recorded during the curing reaction in solution.

The quality of the crystals was good enough to carry out a single-crystal X-ray structure determination. A perspective view of the molecule is shown in Figure 8, the atomic coordinates are listed in Table II, and bond lengths and angles appear in Tables III and IV. The triazine ring is clearly visible in the center of the molecule and appears undistorted. The symmetrical 1,3,5-substitution of the triazine ring minimizes intramolecular steric interactions between the substituent groups.

Table II
Final Atomic Coordinates (Fractional) and B_{eq} (\AA^2) for the
Triazine 9^a

atom	x	y	z	B_{eq}	occ
O(1)	0.1993 (1)	0.3243 (2)	0.25210 (3)	4.90 (6)	
O(2)	0.4550 (1)	-0.1540 (2)	0.27712 (3)	5.58 (7)	
O(3)	0.3737 (1)	-0.0339 (2)	0.16511 (3)	4.69 (6)	
N(1)	0.3240 (1)	0.0899 (2)	0.26633 (4)	4.30 (6)	
N(2)	0.4168 (1)	-0.0878 (2)	0.22098 (4)	4.28 (6)	
N(3)	0.2800 (1)	0.1557 (2)	0.20631 (3)	3.95 (6)	
C(1)	0.2704 (1)	0.1849 (3)	0.24057 (4)	3.90 (7)	
C(2)	0.3953 (1)	-0.0437 (3)	0.25435 (4)	4.19 (7)	
C(3)	0.3547 (1)	0.0175 (3)	0.19880 (4)	3.82 (7)	
C(4)	0.1360 (1)	0.4320 (3)	0.22687 (4)	4.08 (7)	
C(5)	0.1815 (1)	0.5856 (3)	0.20775 (5)	5.07 (9)	
C(6)	0.1168 (2)	0.6921 (3)	0.18434 (5)	5.02 (9)	
C(7)	0.0062 (1)	0.6497 (3)	0.17949 (4)	3.87 (7)	
C(8)	-0.0370 (1)	0.4956 (3)	0.20016 (5)	4.28 (7)	
C(9)	0.0270 (2)	0.3867 (3)	0.22388 (5)	4.44 (8)	
C(10)	0.4337 (1)	-0.1405 (3)	0.31349 (5)	4.51 (8)	
C(11)	0.3899 (2)	-0.3072 (3)	0.32910 (5)	5.5 (1)	
C(12)	0.3773 (2)	-0.3066 (3)	0.36537 (6)	5.6 (1)	
C(13)	0.4075 (1)	-0.1428 (3)	0.38586 (5)	4.67 (8)	
C(14)	0.4507 (2)	0.0240 (3)	0.36860 (5)	5.03 (9)	
C(15)	0.4648 (2)	0.0258 (3)	0.33247 (5)	5.02 (9)	
C(16)	0.3168 (1)	0.0469 (3)	0.13610 (4)	3.99 (7)	
C(17)	0.3032 (2)	-0.0876 (3)	0.10899 (5)	5.06 (9)	
C(18)	0.2542 (2)	-0.0245 (3)	0.07794 (5)	5.3 (1)	
C(19)	0.2166 (2)	0.1728 (3)	0.07331 (4)	4.44 (8)	
C(20)	0.2325 (2)	0.3041 (3)	0.10126 (5)	5.6 (1)	
C(21)	0.2834 (2)	0.2453 (3)	0.13246 (5)	5.4 (1)	
C(22)	-0.0613 (2)	0.7663 (3)	0.15224 (5)	4.65 (8)	
C(23)	-0.1810 (2)	0.6995 (4)	0.15149 (6)	6.6 (1)	
C(24)	-0.0580 (3)	0.9928 (4)	0.16063 (9)	9.0 (2)	
C(25)	-0.0152 (2)	0.7255 (5)	0.11593 (6)	8.5 (2)	
C(26)	0.3925 (2)	-0.1487 (4)	0.42583 (5)	6.2 (1)	
C(27)	0.4561 (5)	-0.325 (1)	0.4418 (1)	9.8 (3)	0.78
C(27A)	0.377 (3)	-0.366 (5)	0.4372 (5)	16 (2)	0.22
C(28)	0.2714 (4)	-0.180 (1)	0.4341 (1)	10.1 (3)	0.78
C(28A)	0.306 (1)	0.303 (4)	0.4336 (3)	10 (1)	0.22
C(29)	0.4302 (7)	0.045 (1)	0.4442 (1)	12.3 (4)	0.78
C(29A)	0.499 (2)	-0.080 (5)	0.4413 (4)	12 (1)	0.22
C(30)	0.1577 (2)	0.2382 (3)	0.03936 (5)	5.6 (1)	
C(31)	0.1681 (3)	0.4650 (4)	0.03286 (7)	8.5 (2)	
C(32)	0.0371 (2)	0.1866 (6)	0.04286 (8)	10.0 (2)	
C(33)	0.2034 (3)	0.1278 (5)	0.00744 (6)	9.5 (2)	

$$^a B_{eq} = (8/3)\pi^2 \sum \sum U_{ij} a_i^* a_j^* (a_i a_j).$$

Table III
Bond Length (\AA) with Estimated Standard Deviations for
the Triazine 9

atom	atom	distance	atom	atom	distance
O(1)	C(1)	1.338 (2)	C(13)	C(14)	1.383 (3)
O(1)	C(4)	1.414 (2)	C(13)	C(26)	1.532 (3)
O(2)	C(2)	1.397 (2)	C(14)	C(15)	1.385 (3)
O(2)	C(10)	1.411 (2)	C(16)	C(17)	1.365 (2)
O(3)	C(3)	1.346 (2)	C(16)	C(21)	1.370 (3)
O(3)	C(16)	1.400 (2)	C(17)	C(18)	1.379 (3)
N(1)	C(1)	1.326 (2)	C(18)	C(19)	1.383 (3)
N(1)	C(2)	1.320 (2)	C(19)	C(20)	1.379 (3)
N(2)	C(2)	1.329 (2)	C(19)	C(30)	1.531 (3)
N(2)	C(3)	1.321 (2)	C(20)	C(21)	1.387 (3)
N(3)	C(1)	1.322 (2)	C(22)	C(23)	1.525 (3)
N(3)	C(3)	1.319 (2)	C(22)	C(24)	1.519 (3)
C(4)	C(5)	1.364 (3)	C(22)	C(25)	1.519 (3)
C(4)	C(9)	1.367 (2)	C(26)	C(27)	1.517 (6)
C(5)	C(6)	1.374 (3)	C(26)	C(27A)	1.50 (3)
C(6)	C(7)	1.389 (2)	C(26)	C(28)	1.529 (5)
C(7)	C(8)	1.387 (2)	C(26)	C(28A)	1.49 (2)
C(7)	C(22)	1.523 (2)	C(26)	C(29)	1.516 (6)
C(8)	C(9)	1.385 (2)	C(26)	C(29A)	1.49 (2)
C(10)	C(11)	1.357 (3)	C(30)	C(31)	1.513 (4)
C(10)	C(15)	1.359 (3)	C(30)	C(32)	1.519 (4)
C(11)	C(12)	1.388 (3)	C(30)	C(33)	1.523 (3)
C(12)	C(13)	1.374 (3)			

The identity of the reaction product from the curing reactions in solution which was characteristic ^{13}C and ^{15}N

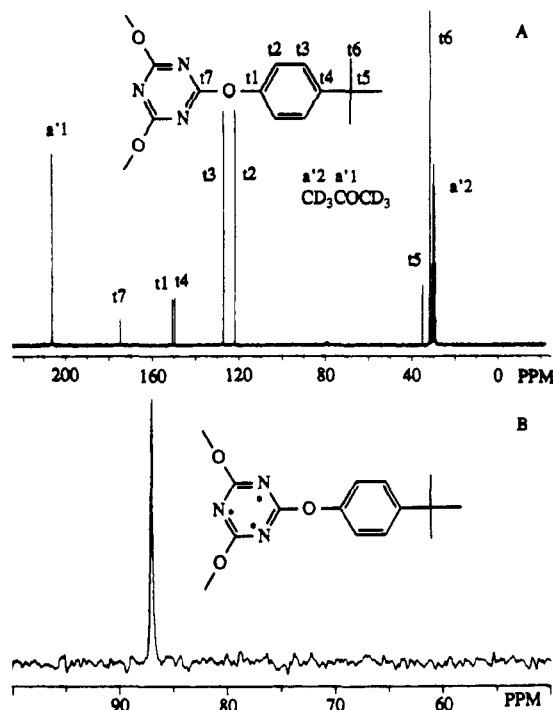


Figure 9. (A) ^{13}C solution NMR spectrum in acetone- d_6 of natural-abundance triazine formed from PTBPCN. (B) ^{15}N NMR solution spectrum in acetone- d_6 of the ^{15}N -enriched triazine formed from PTBPCN.

chemical shifts of $\delta = 174$ and 87 ppm, respectively, is thus clearly established as the postulated triazine ring system (Figure 9), and the importance of this species in the curing process is verified.

Thus, the curing reactions of both cyanate and dicyanate monomers in solution lead to the postulated triazine products with no evidence for observable concentrations of any long-lived intermediate dimer species. In the case of *p*-tert-butylphenyl cyanate monomer, the corresponding triazine has been isolated and fully characterized. Side reactions can occur which involve the reaction of the cyanate group with water impurities in the MEK solvent which could complicate the solution curing process and possibly make the final resin susceptible to attack by water; thus, bulk curing could be preferable. In the following sections we investigate this option in detail.

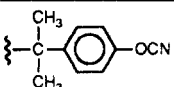
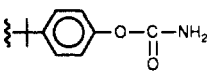
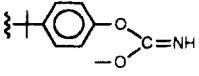
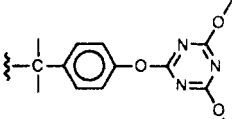
D. Investigations of the Curing Process in the Solid State. In order to probe the curing reactions in the solid state, ^{13}C and ^{15}N solid-state NMR investigations¹⁴ were carried out on the ^{13}C - and ^{15}N -enriched BPACN materials previously described using the chemical shift information obtained from the solution NMR experiments above as reference data. The characteristic chemical shifts of the different functionalities determined in these studies are summarized in Table V.

(1) ^{13}C Solid-State NMR Investigations. BPACN Monomer. Figure 10A shows the ^{13}C CP MAS¹⁵ spectrum of BPACN obtained in natural abundance at 25 MHz (proton frequency 100 MHz) together with the assignment in terms of the molecular structure. Figure 10B is of the same system except that only carbons with no attached protons are detected with the NQS pulse sequence used with the exception of the methyl carbons which are only partly reduced due to the small dipolar interaction due to the methyl group motion.¹⁶ The $-\text{OCN}$ carbon gives rise to three resonances due to residual dipolar coupling to the directly bonded ^{14}N ($I = 1$) quadrupolar nucleus (these are reduced but not eliminated by MAS).¹⁷ Figure 10C is the corresponding dipolar-dephased spectrum of the

Table IV
Bond Angles (deg) with Estimated Standard Deviations for the Triazine 9

atom	atom	atom	angle	atom	atom	atom	angle
C(1)	O(1)	C(4)	118.1 (1)	O(2)	C(10)	C(15)	121.1 (2)
C(2)	O(2)	C(10)	119.6 (1)	C(11)	C(10)	C(15)	121.6 (2)
C(3)	O(3)	C(16)	124.3 (1)	C(10)	C(11)	C(12)	118.7 (2)
C(1)	N(1)	C(2)	112.3 (1)	C(11)	C(12)	C(13)	122.2 (2)
C(2)	N(2)	C(3)	112.1 (1)	C(12)	C(13)	C(14)	116.8 (2)
C(1)	N(3)	C(3)	112.4 (1)	C(12)	C(13)	C(26)	120.5 (2)
O(1)	C(1)	N(1)	113.3 (1)	C(14)	C(13)	C(26)	122.7 (2)
O(1)	C(1)	N(3)	119.1 (1)	C(13)	C(14)	C(15)	121.9 (2)
N(1)	C(1)	N(3)	127.6 (2)	C(10)	C(15)	C(14)	118.8 (2)
O(2)	C(2)	N(1)	119.6 (2)	O(3)	C(16)	C(17)	113.9 (2)
O(2)	C(2)	N(2)	112.8 (2)	O(3)	C(16)	C(21)	125.7 (2)
N(1)	C(2)	N(2)	127.7 (2)	C(17)	C(16)	C(21)	120.3 (2)
O(3)	C(3)	N(2)	111.8 (1)	C(16)	C(17)	C(18)	120.0 (2)
O(3)	C(3)	N(3)	120.3 (1)	C(17)	C(18)	C(19)	122.0 (2)
N(2)	C(3)	N(3)	127.9 (2)	C(18)	C(19)	C(20)	116.2 (2)
O(1)	C(4)	C(5)	120.4 (2)	C(18)	C(19)	C(30)	121.4 (2)
O(1)	C(4)	C(9)	118.2 (2)	C(20)	C(19)	C(30)	122.3 (2)
C(5)	C(4)	C(9)	121.2 (2)	C(19)	C(20)	C(21)	122.9 (2)
C(4)	C(5)	C(6)	119.0 (2)	C(16)	C(21)	C(20)	118.7 (2)
C(5)	C(6)	C(7)	122.4 (2)	C(7)	C(22)	C(23)	112.3 (2)
C(6)	C(7)	C(8)	116.5 (2)	C(7)	C(22)	C(24)	109.6 (2)
C(6)	C(7)	C(22)	120.5 (2)	C(7)	C(22)	C(25)	108.9 (2)
C(8)	C(7)	C(22)	122.9 (2)	C(23)	C(22)	C(24)	107.9 (2)
C(7)	C(8)	C(9)	121.9 (2)	C(23)	C(22)	C(25)	107.3 (2)
C(4)	C(9)	C(8)	119.0 (2)	C(24)	C(22)	C(25)	110.7 (2)
O(2)	C(10)	C(11)	117.1 (2)	C(13)	C(26)	C(27)	110.4 (3)
C(13)	C(26)	C(27A)	109 (1)				
C(13)	C(26)	C(28)	109.4 (2)				
C(13)	C(26)	C(28A)	105.8 (6)				
C(13)	C(26)	C(29)	113.3 (3)				
C(13)	C(26)	C(29A)	105.6 (6)				
C(27)	C(26)	C(28)	108.0 (4)				
C(27)	C(26)	C(29)	107.7 (4)				
C(27A)	C(26)	C(28A)	119 (2)				
C(27A)	C(26)	C(29A)	107 (2)				
C(28)	C(26)	C(29)	107.9 (4)				
C(28A)	C(26)	C(29A)	110 (1)				
C(27A)	C(27)	C(29A)	123 (2)				
C(19)	C(30)	C(31)	111.9 (2)				
C(19)	C(30)	C(32)	108.1 (2)				
C(19)	C(30)	C(33)	111.3 (2)				
C(31)	C(30)	C(32)	108.5 (3)				
C(31)	C(30)	C(33)	107.7 (2)				
C(32)	C(30)	C(33)	109.2 (2)				

Table V
Characteristic ^{13}C and ^{15}N Chemical Shift Values of the Functionalities from the Cyanate Group Identified from the Solution Curing Reactions

compound	^{13}C from TMS (ppm)	^{15}N from neat formamide (ppm)
	109	52
	156	-40
	159.5	43
	174	87

^{13}C -enriched monomer and shows only these three signals as anticipated. Figure 10D shows the CP MAS spectrum, with sidebands removed by the TOSS sequence,¹⁸ of the ^{13}C -enriched monomer obtained at 100.6 MHz (400 MHz for protons). The spectrum is much cleaner, as the three resonances have become almost degenerate because the

Table VI
Crystallographic Data for BPACN

compound	$\text{Me}_2\text{C}(\rho\text{-NCOC}_6\text{H}_4)_2$
formula	$\text{C}_{17}\text{H}_{14}\text{N}_2\text{O}_2$
fw	278.31
crystal system	monoclinic
space group	$P2_1/a$
a , Å	10.072 (2)
b , Å	11.410 (2)
c , Å	13.351 (3)
β , deg	108.49 (2)
V , Å ³	1455 (1)
Z	4
T , °C	21
ρ_c , g/cm ³	1.270
λ , Å	0.71069
$\mu(\text{Mo K}\alpha)$, cm ⁻¹	0.79
transmission factors	0.96–1.00
$R(F_0)$	0.038
$R_w(F_0)$	0.043

quadrupolar coupling is greatly reduced at the higher frequency. Further spectra of this system were obtained mainly at 400 MHz.

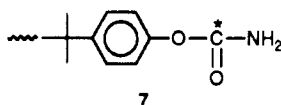
Solid from Solution Polymerization. Parts A and B of Figure 11 show the ^{13}C CP MAS TOSS spectra of the solid obtained by evaporation of the solvent from the solution polymerization described previously. There is an intense signal at approximately 174 ppm assigned to the triazine ring carbons and a second signal at approx-

Table VII
Final Atomic Coordinates (Fractional) and B_{eq} (\AA^2) for BPACN^a

atom	x	y	z	B_{eq}
O(1)	0.6290 (2)	0.7298 (2)	0.5398 (1)	6.5 (1)
O(2)	0.0664 (2)	0.0994 (2)	0.1896 (2)	6.7 (1)
N(1)	0.6805 (3)	0.9327 (3)	0.5819 (3)	10.0 (2)
N(2)	0.1602 (3)	-0.0415 (2)	0.0952 (3)	8.6 (2)
C(1)	0.1644 (2)	0.5929 (2)	0.1848 (2)	4.0 (1)
C(2)	0.0261 (3)	0.6547 (2)	0.1776 (2)	5.8 (1)
C(3)	0.2080 (3)	0.6329 (2)	0.0898 (2)	5.2 (1)
C(4)	0.2827 (2)	0.6291 (2)	0.2843 (2)	3.9 (1)
C(5)	0.4001 (3)	0.5586 (2)	0.3247 (2)	4.6 (1)
C(6)	0.5141 (3)	0.5933 (2)	0.4078 (2)	4.9 (1)
C(7)	0.5076 (3)	0.6996 (2)	0.4518 (2)	4.6 (1)
C(8)	0.3965 (3)	0.7725 (2)	0.4177 (2)	5.2 (1)
C(9)	0.2838 (3)	0.7364 (2)	0.3327 (2)	4.9 (1)
C(10)	0.1424 (2)	0.4601 (2)	0.1847 (2)	4.0 (1)
C(11)	0.0766 (3)	0.4101 (2)	0.2512 (2)	5.9 (1)
C(12)	0.0537 (3)	0.2909 (3)	0.2520 (2)	6.5 (1)
C(13)	0.0970 (3)	0.2214 (2)	0.1858 (2)	4.9 (1)
C(14)	0.1627 (3)	0.2648 (2)	0.1205 (2)	4.8 (1)
C(15)	0.1850 (2)	0.3849 (2)	0.1201 (2)	4.5 (1)
C(16)	0.6532 (3)	0.8390 (3)	0.5601 (3)	6.4 (2)
C(17)	0.1193 (3)	0.0261 (3)	0.1389 (3)	6.0 (1)

$$^a B_{eq} = (8/3)\pi^2 \sum \sum U_{ij} a_i^* a_j^* (a_i a_j).$$

imately 157 ppm corresponding roughly to the solution signal assigned to compound 7. It should be noted that



these spectra are not quantitative and that the signals due to species such as 7 would be greatly enhanced by the cross-polarization process, as there are two protons only two bonds away in this molecular structure.

Solid-State Curing. Figure 11C shows the ^{13}C solid-state spectrum of the product from the bulk curing (no catalyst) of the ^{13}C -labeled BPACN monomer sample for 15 min at 250 °C. The spectrum is remarkably clean, showing a single major resonance at 174 ppm with no indication of substantial amounts of unreacted monomer or product (7). This would appear to be a very viable polymerization process and remarkably efficient.

(2) ^{15}N Solid-State NMR Investigations. BPACN Monomer. Figure 12A shows the high-resolution solid-state ^{15}N NMR spectrum of the labeled BPACN monomer at 40.6 MHz (proton frequency 400 MHz, primary shift referenced to neat formamide). There are two sharp resonances, indicating at site symmetry lower than the symmetry of the isolated gas-phase molecule (also shown by the two methyl resonances in the ^{13}C spectrum of BPACN, Figure 10A).

Solid from Solution Curing. Parts B–D of Figure 12 show ^{15}N spectra of the solid obtained from the solution polymerization by evaporation of the solvent as a function of the contact time used for $^1\text{H}/^{15}\text{N}$ cross-polarization. The lowest field resonance can be assigned to the triazine ring nitrogens, but there is substantial intensity at higher field due to other species. However, as before, these will be greatly enhanced by the cross-polarization process. Because the two protons are directly attached to the ^{15}N nucleus in this case and this interaction depends on $1/r^6$, this will be an extreme effect and the spectrum in Figure 3B bears little relation to the actual concentrations of the different species. At longer contact times, this is less important and Figure 12C is a better reflection of the two concentrations of the different species. That the higher field components all have directly bonded protons is

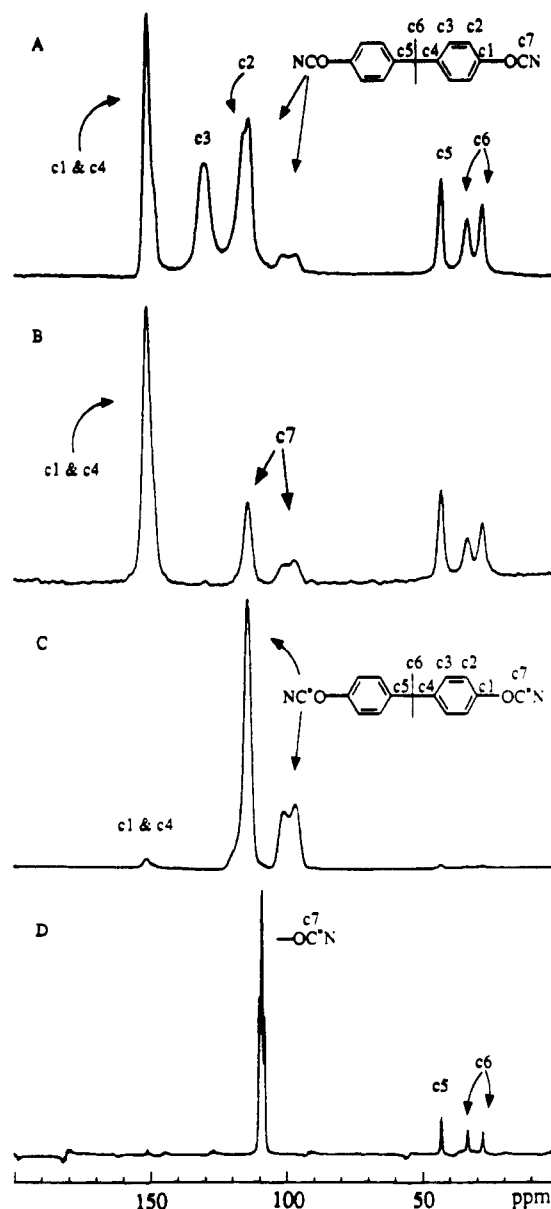


Figure 10. Solid-state ^{13}C CP MAS NMR spectra of (A) natural-abundance BPACN monomer at 25.2 MHz, (B) natural-abundance BPACN monomer using the NQS sequence at 25.2 MHz, (C) the ^{13}C -enriched BPACN monomer using the NQS sequence at 25.2 MHz, and (D) the ^{13}C -enriched BPACN monomer using the TOSS sequence at 100.6 MHz.

confirmed by Figure 12D which detects only signals from ^{15}N nuclei with no attached protons. Only a single resonance is observed here, corresponding to the triazine ring nitrogens.

Solid-State Curing. Figure 13A shows the high-resolution solid-state ^{15}N spectrum of the product from a solid-state curing of the ^{15}N -labeled BPACN monomer under conditions identical to those used for the ^{13}C -labeled monomer previously discussed (bulk curing, no catalyst, 15 min at 250 °C). The spectrum is much cleaner than those from the solution polymerization "product", but as before the "non-triazine" signals are very greatly enhanced. Figure 13B, which shows only non-proton-bearing nitrogens, indicates as before that the other species (thought to be 7) has directly attached protons.

(3) Quantitative Investigation of Solid-State BPACN Curing. From the previous sections, the curing of BPACN appears to be an efficient process, especially when carried out on the neat material where side reactions with water are minimized. An attempt was made to

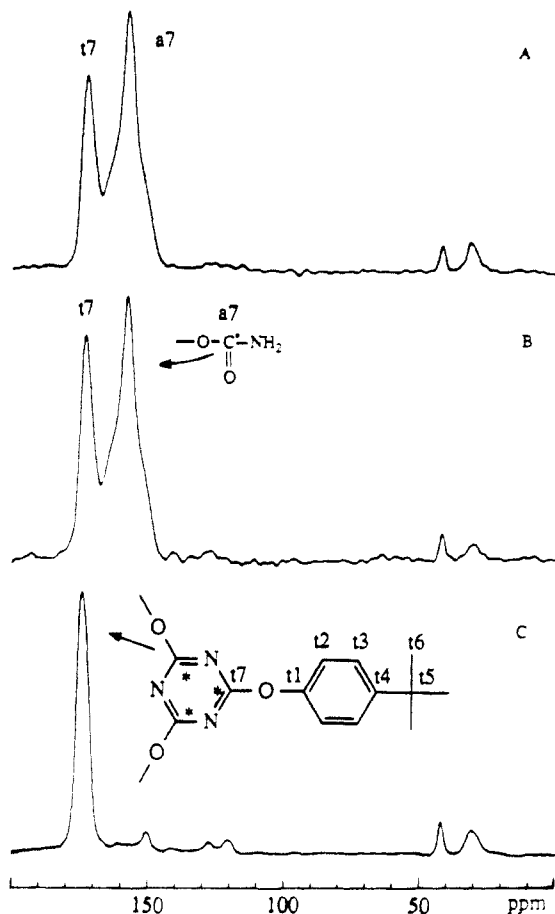


Figure 11. ^{13}C solid-state CP MAS TOSS NMR spectra at 100.6 MHz of (A) the solid sample obtained by evaporation of the solvent after curing the ^{13}C -enriched BPACN in MEK and acetone- d_6 with 200 ppm zinc octanoate as catalyst, (B) the same sample as in A except that the NQS sequence was used, and (C) the solid sample obtained from bulk curing of the ^{13}C -enriched BPACN at 250 °C for 15 min.

quantify this and also to relate the ^{13}C and ^{15}N spectra directly to each other by investigating a BPACN resin made up of 50% ^{15}N -enriched and 50% ^{13}C -enriched BPACN precursor monomers. This was cured for 15 min at 250 °C.

Both ^{13}C and ^{15}N CP MAS spectra were obtained at high field (400-MHz proton frequency). For the ^{13}C spectra it is important to eliminate the dipolar coupling to ^{14}N which will still occur in 50% of the OCN groupings, and in the ^{15}N spectra additional sensitivity is gained. The disadvantage of the high field is the large chemical shift anisotropies which occur, giving rise to large numbers of spinning sidebands. In the more qualitative studies presented in the previous sections, these were eliminated using the TOSS pulse sequence. However, for quantitative data it is important that their intensity be taken into account. From a knowledge of where other resonances could occur, a spinning rate was chosen to avoid overlap of spinning sidebands and isotropic resonances. As noted previously, because the side products contain protons in close proximity to the labeled nuclei being observed, the spectra are sensitive to the contact time used for the cross-polarization step. A complete variation of contact times was carried out for both series of experiments.

The series of spectra shown in Figure 14 are the variation of contact time for the ^{13}C -labeled component. Only at very short contact times is there any indication of resonances due to other species. The contributions are small, and it was not considered worthwhile to try to estimate them due to contributions from natural-abun-

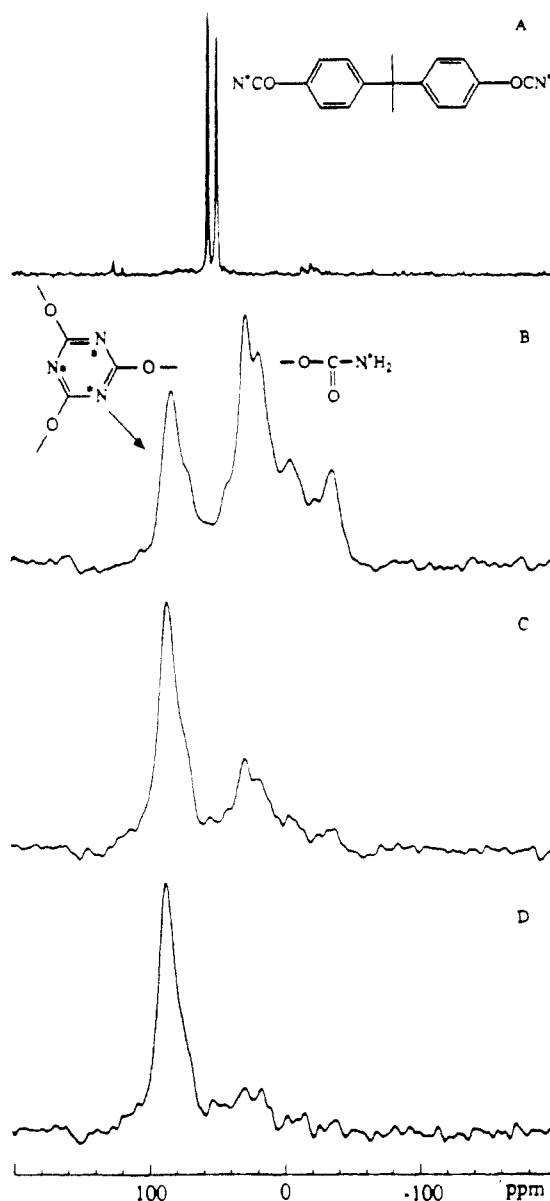


Figure 12. ^{15}N solid-state CP MAS TOSS NMR spectra at 40.6 MHz of (A) the ^{15}N -enriched BPACN monomer, (B) the solid sample obtained by evaporation of the solvent after curing the ^{15}N -enriched BPACN in MEK and acetone- d_6 with 200 ppm zinc octanoate as catalyst and a contact time of 1 ms, and (C and D) spectra of the same sample as in B, except with contact times of 5 and 10 ms, respectively.

dance resonances. Quantitation will be more reliable from ^{15}N data. The maximum intensity of the ^{13}C spectra occurs at about 5 ms, after which all of the signals decay due to the proton $T_{1\rho}$ process. A spectrum obtained at this contact time using the TOSS sequence (Figure 15A) indicates that there are negligible contributions to the spectrum from other species. Thus, the very high efficiency of the solid-state curing reaction is verified.

Figures 15B and 16 show the ^{15}N spectra obtained from an analogous series of experiments on the same sample. In the case of ^{15}N , the side products have protons directly attached to the ^{15}N nucleus, greatly enhancing their contribution to the spectra. In addition, there is no natural-abundance contribution to the spectrum. From an analysis of these data, the total contribution of species other than triazine to the spectrum is estimated to be less than 2%.

The solid-state NMR spectra thus indicate that the solid cured resin is composed mainly of triazine ring linkages, whether the reaction is carried out "neat" or the product

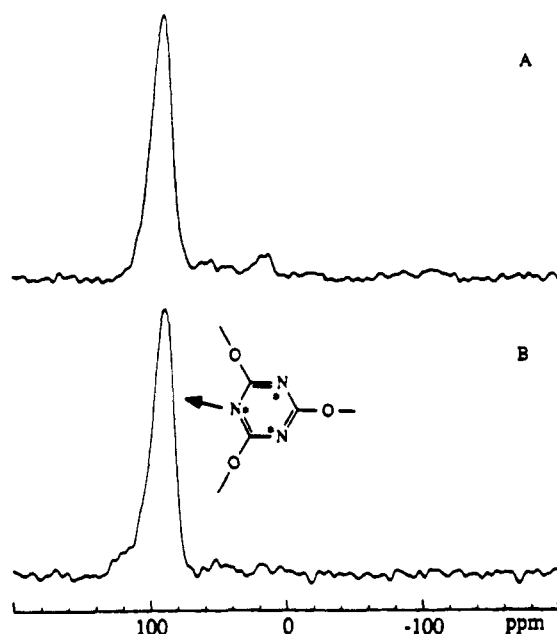


Figure 13. Solid-state ^{15}N CP MAS NMR spectra of the resin obtained after bulk curing the ^{15}N -enriched BPACN at $250\text{ }^{\circ}\text{C}$ for 15 min: (A) with TOSS sequence; (B) with TOSS/NQS sequence.

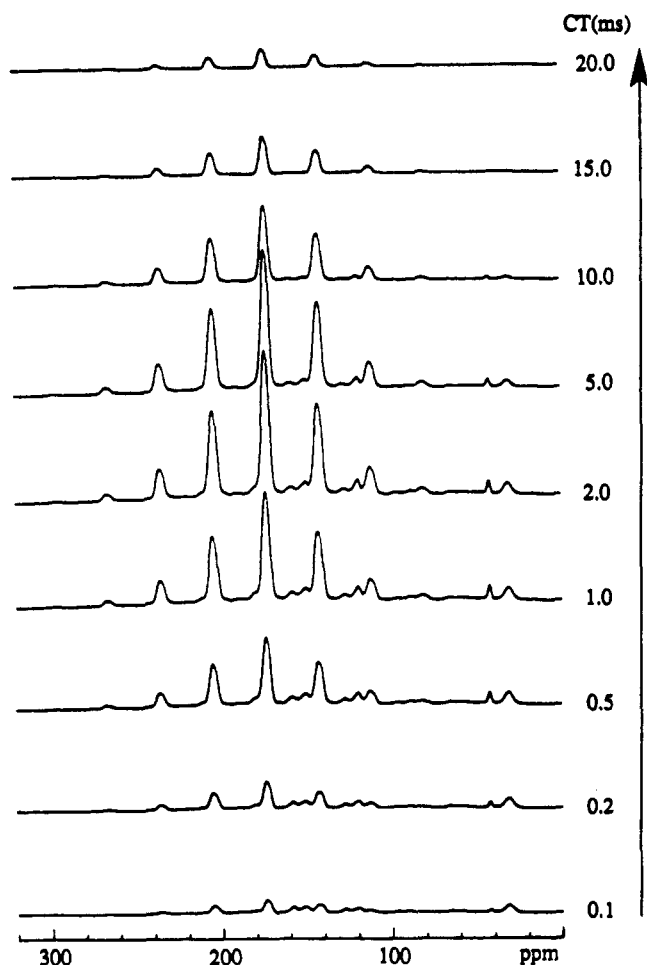


Figure 14. Series of the ^{13}C solid-state NMR spectra with variation of the contact time (CT) using the CP MAS sequence only without sideband suppression. The sample resin was obtained by bulk curing a mixture of 50% ^{13}C -enriched and 50% ^{15}N -enriched BPACN monomers for 15 min at $250\text{ }^{\circ}\text{C}$.

is obtained by precipitation from a solution polymerization. A catalyst is not necessary for the curing reaction, and side products come mainly from reaction with water present in the solvent mixture. *The reaction is very*

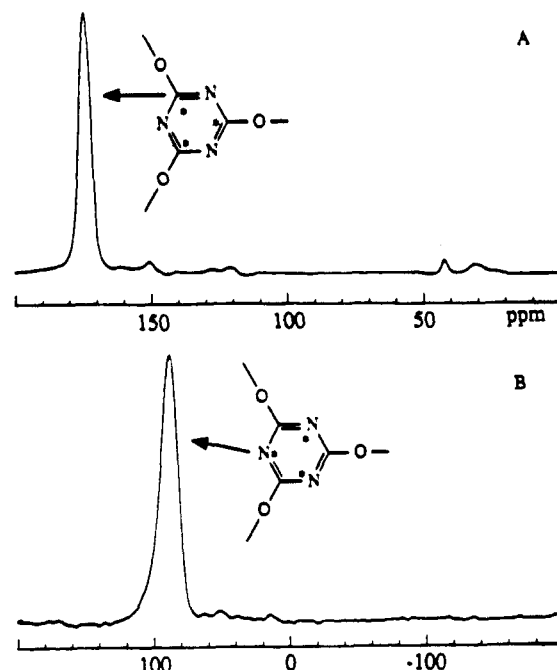


Figure 15. Solid-state CP MAS TOSS NMR spectra of the same resin sample as for Figure 14 with $\text{CT} = 5\text{ ms}$. (A) ^{13}C spectrum; (B) ^{15}N spectrum.

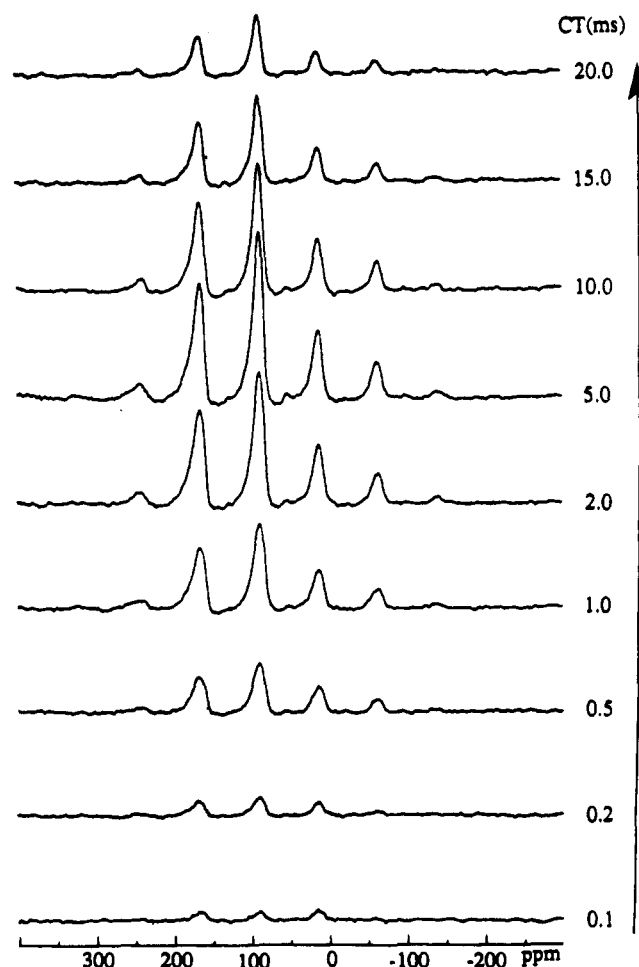


Figure 16. Series of ^{15}N solid-state NMR spectra with contact time variation using the CP MAS sequence only without sideband suppression. The resin sample was the same as for Figure 14. *efficient*, especially when neat monomer is used, some 98% of the cyanate functionalities being converted to triazine rings in these experiments.

E. Crystal and Molecular Structure of BPACN. Thus, the cyanate to triazine conversion is confirmed as

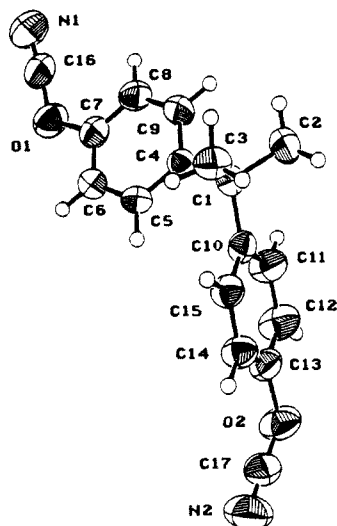


Figure 17. Molecular structure of BPACN from the single-crystal X-ray diffraction study showing the numbering of the atoms (Table VII).

the basic curing reaction, and it has been demonstrated that triazine ring formation proceeds without the accumulation of substantial amounts of intermediate dimeric species, the only other products being impurities which come from the reaction of the cyanate group with water present in the solvent. In the case of thermal curing of the neat resin, the reaction is found to be remarkably efficient, over 98% of the cyanate groups present being converted to triazine rings. In many ways, this high efficiency of the curing reaction of neat BPACN is surprising: The Bisphenol A moiety is quite rigid, and a very rigid cross-linked framework will be formed which one would think would make it difficult to cure the resin anywhere near completion.

To try to better understand the factors involved in this process, crystals of BPACN suitable for single-crystal X-ray diffraction studies were obtained by recrystallization from cyclohexane solution and the crystal and molecular structures determined by single-crystal X-ray diffraction.

The final positional parameters from the refinement are given in Table III with the numbering of the molecular structure shown in Figure 17. In the crystal, the two pseudo planes of symmetry through C₁ which exist in solution due to rotation about the C₁-C₄, C₁-C₁₀, C₁₃-O₂, and C₇-O₁ bonds are removed. All of the atoms in the molecule are not unique, and in principle all should give separate signals in the high-resolution solid-state NMR experiments although in practice not all differences will be large enough to be resolved. This lack of molecular symmetry in the crystal explains the double resonances for the two methyl groups in the solid-state ¹³C NMR spectra and the two nitrogen (OCN) resonances in the analogous ¹⁵N spectra of this system as previously reported.

More interesting in the context of the curing reactions of this monomer is the crystal structure depicted in Figures 18 and 19. Figure 18 shows the arrangement of the molecules in the unit cell which indicates clearly that *interactions between the cyanate groups are the dominant factors controlling the formation of the lattice structure*. The interactions all involve four cyanate groups on different molecules. Between two of these there are strong and symmetrical C₁₇-...N₂ interactions forming a four-membered ring and the remaining two cyanate groups each interact via an N₁-...O₂ interaction to one of the two oxygens in the four-membered ring. These intermolecular contacts are given in Table VIII. Thus, at least in the

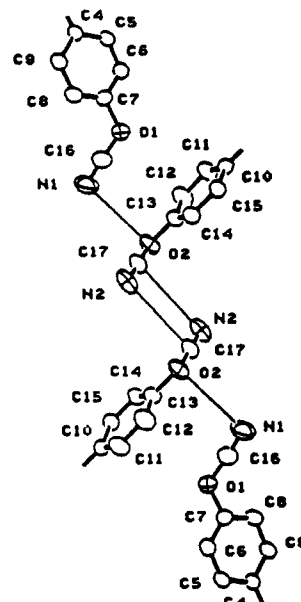


Figure 18. Perspective view of part of the unit cell contents from the crystal structure of BPACN showing the intercyanate interactions (see Table VIII).

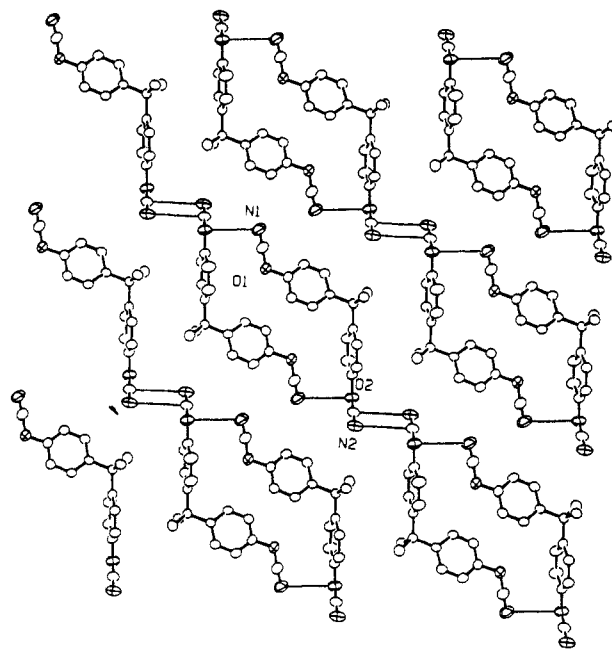


Figure 19. Plane through the three-dimensional network formed by the intermolecular intercyanate interactions. The BPACN molecules are cyanate-connected to form parallel strings throughout the structure.

Table VIII
Intermolecular Bonding Interactions between Cyanate Groups in the BPACN Structure

atom	atom ^a	distance (Å)
O(2)	N(1)'	3.318 (4)
N(2)	C(17)''	3.484 (4)
N(2)	N(2)'	3.546 (6)

^a The prime and double prime refer to symmetry operations 1 - x, 1 - y, 1 - z and -x, -y, -z, respectively.

solid state, the functionalities needed for the curing reaction depicted in eq 1 are all in close proximity and strongly interacting. Figure 19 illustrates how these intercyanate group interactions form a complete three-dimensional structure, the lattice being made up of parallel strings of cyanate-bonded molecules.

Although melting the sample will destroy the perfection of this ordering pattern, it is expected that strong intercyanate group interactions will still occur and substantial local ordering may persist in the melt. These results form a guide for modeling the curing process, and the high efficiency of the neat curing reaction becomes more understandable as does the reduced curing efficiency in the presence of solvents with strongly polar groups where competitive interactions with the cyanate groups can occur. If other diacyanates or derivatives are considered as potential resin systems, it might be worthwhile to carry out a single-crystal X-ray structural investigations to check whether the changes in molecular structure have destroyed the very strong intercyanate interactions which are present in the case of BPACN.

Acknowledgment. We acknowledge the support of the Natural Sciences and Engineering Research Council of Canada in the form of Operating and Equipment Grants (CAF). This project was supported by IBM Corp., Systems Technology Division.

Supplementary Material Available: Tables of hydrogen atom parameters, anisotropic thermal parameters, torsion angles, intermolecular contacts, least-squares planes, and crystallographic data for 9 and BPACN (25 pages); listings of measured and calculated structure factor amplitudes for 9 and BPACN (34 pages). Ordering information is given on any current masthead page.

References and Notes

- (1) Wang, D. W. In *Electronic Packaging Materials Science III*. Jaccodine, R., Jackson, K. A., Sundahl, R. C., Eds. *Natl. Res. Soc. Symp. Proc.* 1988, 108, 125.

- (2) Shimp, D. A.; Christenson, J. R.; Ising, S. J. *Proc. 34th Intl. SAMPE Symp.* 1989, 34, 222.
- (3) Christie, F. R.; Papathomas, K. I.; Wang, D. W. U.S. Patent 4,999,699, March 12, 1991.
- (4) Bogan, G. W.; Lyssy, M. E.; Monnerat, G. A.; Woo, E. P. *SAMPE J.* 1988, 24, 19.
- (5) Bauer, M.; Bauer, J.; Kuhn, G. *Acta Polym.* 1986, 37, 715.
- (6) Shimp, D. A. *SAMPE Q.* 1987, 19, 41.
- (7) Fang, T. *Macromolecules* 1990, 23, 4553.
- (8) Frye, J. S.; Maciel, G. E. *J. Magn. Reson.* 1982, 48, 125.
- (9) TEXSAN/TEXRAY structure analysis package which includes versions of the following: MTHRIL, integrated direct methods, by C. J. Gilmore; DIRDIF, direct methods for difference structures, by P. T. Beurskens; ORFLS, full-matrix least-squares, and ORFFE, function and errors, by W. R. Busing, K. O. Martin, and H. A. Levy; ORTEP II, illustrations, by C. K. Johnson.
- (10) *International Tables for X-Ray Crystallography*; Kynoch Press: Birmingham, U.K. (present distributor D. Reidel: Dordrecht, The Netherlands), 1974; Vol. IV, pp 99-102 and 149.
- (11) Hartman, W. W.; Dreger, E. E. *Org. Synth.* 1931, 11, 1931.
- (12) (a) Grigat, E.; Pütter, R. *Chem. Ber.* 1964, 97, 3012. (b) Cozzens, R. F.; Walter, P. J. *J. Appl. Polym. Sci.* 1987, 34, 601. (c) Martin, D.; Bauer, M. *Org. Synth.* 1983, 61, 35.
- (13) Grigat, E.; Pütter, P. *Chem. Ber.* 1964, 97, 3018.
- (14) A general account of the application of solid-state NMR techniques in chemistry is given in: Fyfe, C. A. *Solid State NMR for Chemists*; CFC Press: Guelph, Canada, 1984.
- (15) Schaefer, J.; Stejskal, E. O. *J. Am. Chem. Soc.* 1976, 98, 1031.
- (16) Opella, S. J.; Frey, M. H. *J. Am. Chem. Soc.* 1979, 101, 5854.
- (17) (a) Zumbulyadis, N.; Henrichs, P. M.; Young, R. H. *J. Chem. Phys.* 1981, 75, 1603. (b) Bohm, J.; Fenzyke, D.; Pfeiffer, H. *J. Magn. Reson.* 1983, 55, 197. (c) Naito, A.; Ganapathy, S.; McDowell, C. A. *J. Chem. Phys.* 1981, 74, 5393. (d) Naito, A.; Ganapathy, S.; McDowell, C. A. *J. Magn. Reson.* 1982, 48, 367.
- (18) Dixon, W. T. *J. Magn. Reson.* 1982, 49, 341.

Registry No. 1, 1156-51-0; PTBPCN, 1132-16-7.